Supplementary Material of "Universal microstructure and mechanical stability of jammed packings"

Patrick Charbonneau,[1,2] Eric I. Corwin,[3] Giorgio Parisi,[4] and Francesco Zamponi[5]

[1]*Department of Chemistry, Duke University, Durham, North Carolina 27708, USA*
[2]*Department of Physics, Duke University, Durham, North Carolina 27708, USA*
[3]*Department of Physics, University of Oregon, Eugene, Oregon 97403, USA*
[4]*Dipartimento di Fisica, Sapienza Universitá di Roma, INFN, Sezione di Roma I, IPFC – CNR, P.le A. Moro 2, I-00185 Roma, Italy*
[5]*LPT, École Normale Supérieure, UMR 8549 CNRS, 24 Rue Lhomond, 75005 France*

APPENDIX A: NUMERICAL SIMULATIONS

Molecular dynamics simulations of HS and SS energy minimizations of N=2^{18} spheres in d=3, N=8000 in $4 \leq d \leq 9$, and at least N=2^{14} in d=10 are performed under periodic boundary conditions. For $d = 3$, the choice of a very large system is motivated by the need of reducing the statistical noise in the intermediate scaling regime for Fig. 3 of the main text. The $d > 3$ system sizes chosen ensure that even when the system is at its densest the box edge remains larger than 2σ, which prevents a particle from ever having two direct contacts with another one. There are strong reasons to believe that although relatively small these N nonetheless provide a reliable approximation of bulk behavior. First, with increasing d the largest diagonals of the simulation box are $\sqrt{d}$ larger than the box edge. Second, correlations of the fluid structure are expected to decrease very quickly with increasing d [1, 2], and correspondingly finite-size effects are reduced. The validity of these rationalizations, which are consistent with the decorrelation property of high d sphere packings [3], have been satisfactorily tested in $d = 8$ in Ref. [4].

1. Hard Sphere LS Compressions

Event-driven HS simulations are performed at thermostated inverse temperature β for spheres of mass m, starting from random configurations in the limit $\sigma \to 0$. Time has units of $\sqrt{\beta m \sigma^2}$ [2, 4], but all dimensional quantities are expressed in units such that $\beta = 1$ and $m = 1$. The reduced pressure $p = \beta P/\rho$, with $\rho = N/V$ for pressure P, diverges at the jamming packing fraction φ_p^γ as $p \sim |\Delta\varphi|^{-1}$ with $\Delta\varphi = \varphi - \varphi_p^\gamma$ [5]. Crystallization in $d > 3$ is strongly suppressed, so access to deeply supersaturated starting configurations can be attained via the slow growth rate $\gamma = \dot{\sigma} = 3 \times 10^4$ [2, 6]. In $d = 3$, where the crystallization of monodisperse hard spheres is relatively rapid for moderately high packing fractions, $\gamma = 10^{-2}$ is employed up to $p = 10^3$, but the slow compression rate is used afterwards. The force between particles in high p configurations is measured from the rate of momentum exchange between pairs of particles in simulations with $\gamma = 0$. These measurements are made over at least 10^4 collisions per particle.

2. Soft Sphere Energy Minimizations

The harmonic SS energy is $E(X, \sigma) = \sum_{i>j} v(|\vec{r}_i - \vec{r}_j|)$ with $X = \{\vec{r}_i\}$ and $v(r) = \epsilon(\sigma - r)^2\theta(\sigma - r)$. Units are chosen such that $\epsilon = 1$. We start from random sphere configurations $X_+ = X_-$ and use σ_- and σ_+ that bracket the jamming point, i.e., $E(X_-, \sigma_-) = 0$, $E(X_+, \sigma_+) > 0$. Jamming is identified as the onset of non-zero energy, iteratively determined using a bisection method. At each iteration, an intermediate value σ_m is chosen, and the energy at σ_m is minimized via conjugate-gradient (CG) minimization starting from either X_+ (from above) or X_- (from below). The configuration obtained after minimization X_m then substitutes $(X_+, \sigma_+) = (X_\mathrm{m}, \sigma_\mathrm{m})$ if $E(X_\mathrm{m}, \sigma_\mathrm{m}) > 0$, or $(X_-, \sigma_-) = (X_\mathrm{m}, \sigma_\mathrm{m})$ if $E(X_\mathrm{m}, \sigma_\mathrm{m}) = 0$. The procedure stops when either of two conditions is satisfied: the energy per particle $E(X_+, \sigma_+)/N$ falls below 10^{-20}, corresponding to typical overlaps of the order of 10^{-10}; or the change in $E(X_+, \sigma_+)$ from one minimization step to the next is less than the bound set by double precision arithmetic, i.e., $10^{-8}E$. The final value of σ_- defines the final packing fraction $\varphi_e^\uparrow$ in the procedure from below and σ_+ that of $\varphi_e^\downarrow$ in the procedure from above.

3. Rattler Analysis

The rattlers are self-consistently determined by identifying the number of particles with fewer than $d + 1$ neighbors within a distance cutoff for the smallest $|\Delta\varphi|$ obtained by a given approach to jamming. In HS, a cutoff of $\sigma(1 + 100/p)$ is used, which roughly corresponds to a cutoff of $\sigma(1 - \varepsilon/100)$ for SS, where the scaling variable $\varepsilon = \sqrt{e\,d/2}$. This cutoff slightly overestimates the number of rattlers at jamming, but the rapid diminution of the fraction of rattlers with d (Supplementary Fig. 4) guarantees the robustness of the results.

4. Extraction of the jamming density

Following [4], for each compression run at fixed γ we perform a linear fit of the line $1/p$ vs φ with $p \gtrsim 50$. The point where the linear fit vanishes, indicating infinite

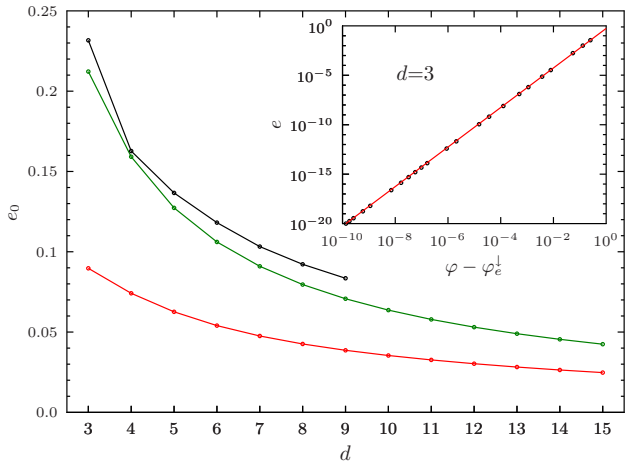

Supplementary Figure 1: The prefactor of energy $e = e_0[(\varphi - \varphi_e^\downarrow)/\varphi_e^\downarrow]^2$ from numerics (black curve) and from G-RT (red curve, bare data; green curve, corrected data, see Sec. C 2 and [7, Section VI.B]). (inset) The scaling $e = e_0[(\varphi - \varphi_e^\downarrow)/\varphi_e^\downarrow]^2$ upon approaching $\varphi_e^\downarrow$ from above for $d = 3$, with $\sigma_- = 0$ and $\sigma_+ \to \infty$. Points are numerical data and the line is a quadratic fit used to extract e_0 (the value of $\varphi_e^\downarrow$ is obtained by imposing visually the best alignment of the data).

pressure, defines φ_p^γ for this given run. Next, for a fixed dimension, we fit $\varphi_p^\gamma = \varphi_p^{\gamma\to 0} + A\sqrt{\gamma}$ to extrapolate the jamming density at $\gamma \to 0$.

For the energy minimization protocol, when approaching jamming from above, the jamming density can be obtained by accurately fitting the energy data with $e = e_0[(\varphi - \varphi_e^\downarrow)/\varphi_e^\downarrow]^2$ (inset in Supplementary Fig. 1). We focus in particular on minimization runs performed with initial $\sigma_- = 0$ and $\sigma_+ \to \infty$, which in practice correspond to taking the largest σ_+ at which no variation of $\varphi_e^\downarrow$ is detected. The associated prefactor e_0 can then be compared with the prediction from G-RT. A good agreement is obtained when the correction discussed in [7, Section VI.B] is taken into account (Supplementary Fig. 1).

Note that $\varphi_p^{\gamma\to 0}$ and $\varphi_e^{\max}$ are quite close to each other. They indicate the best packing density that can be reached using our two different compression protocols. Note that according to G-RT both should be smaller than the maximal packing density of glassy states, called glass close packing $\varphi_{\rm GCP}$. According to the theory, it is very unlikely that packings at $\varphi_{\rm GCP}$ can be produced in polynomial time, hence it is expected that both $\varphi_p^{\gamma\to 0}$ and $\varphi_e^{\max}$ are smaller than $\varphi_{\rm GCP}$.

APPENDIX B: SCALING FUNCTIONS

1. Structure Scaling Analysis

When approaching jamming with protocol *(i)*, $Z(r) = 0$ for $r < \sigma$, and for $r \geq \sigma$, p parametrizes the scaling function for $Z(r \geq \sigma)$. A first scaling regime $r - \sigma \sim p^{-1}$ sees $Z(r)$ grow from 0 to the average number of "contacts" $\overline{z}$ as

$$Z(r) = \overline{z}\mathcal{Z}_-[(r-\sigma)p/\sigma] \tag{B1}$$

with $\mathcal{Z}_-(x) \sim 1 - Cx^{-1-\theta}$ when $x \to \infty$ for a constant C [5]. Force-bearing contacts are only observed at jamming proper, but their signature develops asymptotically. A second regime for finite $r - \sigma$ has

$$Z(r) = \overline{z} + C'(r-\sigma)^{1-\alpha}\ , \tag{B2}$$

where C' is a constant. At jamming, these nearly touching "quasi-contacts" carry no force. For large r, a trivial regime develops independently of $|\Delta\varphi|$ (Sec. B 3). Matching the first two scaling regimes implies the existence of an additional intermediate regime $\mathcal{H}_-$ for $r - \sigma \sim p^{-\mu}$

$$Z(r) = \overline{z} + p^{\nu-\mu}\mathcal{H}_-[(r-\sigma)p^\mu/\sigma] \tag{B3}$$

with $\mu < 1$ and $\nu < \mu$. Consistency then requires that $\mathcal{H}_-(x \to 0) \propto -x^{-1-\theta}$ and $\mathcal{H}_-(x \to \infty) \propto x^{1-\alpha}$ with scaling relations $\nu = \alpha\mu$ and $\mu = (1+\theta)/(2+\theta-\alpha)$.

When approaching jamming with protocol *(ii)* from above, the remaining overlaps provide a scaling variable $\varepsilon = \sqrt{e\,d/2} \propto |\Delta\varphi|$ [7]. In spite of the very different preparation protocol, similar structural regimes are identified. In the $r < \sigma$ contact regime, $Z(r)$ grows from 0 to $\overline{z}$ by a universal scaling function

$$Z(r) = \overline{z}\mathcal{Z}_+[(\sigma-r)\varepsilon^{-1}/\sigma] \tag{B4}$$

with $\mathcal{Z}_+(x) \sim 1 - C''x^{1+\theta}$ when $x \to 0$ for a constant C''. For $r > \sigma$, here again

$$Z(r) = \overline{z} + C'(r-\sigma)^{1-\alpha}\ , \tag{B5}$$

hence the two regimes must be matched by an intermediate scaling function $\mathcal{H}_+$ for $r - \sigma \sim \varepsilon^\mu$

$$Z(r) = \overline{z} + \varepsilon^{\mu-\nu}\mathcal{H}_+[(r-\sigma)\varepsilon^{-\mu}/\sigma] \tag{B6}$$

with $\mu > 1$ and $\nu < 1$. Consistency here requires that $\mathcal{H}_+(x \to -\infty) \propto -|x|^{1+\theta}$ and $\mathcal{H}_+(x \to \infty) \propto x^{1-\alpha}$ with $\nu = \alpha\mu$ and $\mu = (1+\theta)/(\alpha+\theta)$.

In both cases, the exponents α and θ are determined by collapsing the numerical results using this scaling form, which was repeated for different systems. This constraint leaves a relatively small uncertainty on the final value, which provides the error bar.

2. Force Scaling Analysis

When HS approach jamming, the cumulative force distribution $G(f)$ approaches a scaling function defined by $G(y\overline{f}) \to \mathcal{G}_-(y)$. The relation between the scaling functions $\mathcal{Z}_-(x)$ and $\mathcal{G}_-(y)$ suggested in Ref. [5]

$$\mathcal{Z}_-(x) = 1 - x\int_0^\infty dy\,\mathcal{G}_-(y)\,e^{-xy} \tag{B7}$$

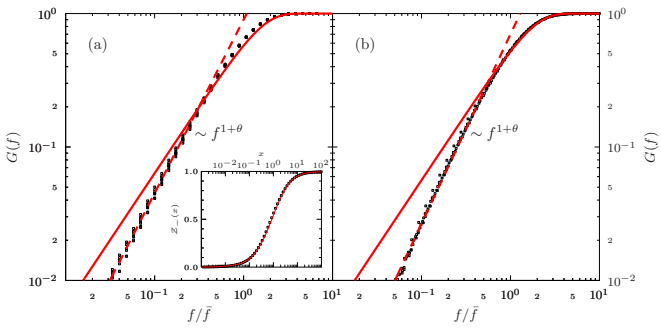

Supplementary Figure 2: Cumulative force distribution $G(f)$ in d=3–10 **(a)** for HS with $\theta = 0.28(3)$ and **(b)** for SS with $\theta = 0.42(2)$. The force distribution in higher d is essentially the same as in $d = 3$ and the high force behavior agrees equivalently well with the G-RT predictions. The exponents extracted from the small force tail are also numerically indistinguishable. (inset) Test of Eq. (B7) from the numerical results for $\mathcal{Z}_-(x)$ (points) and plugging the numerical $G(f)$ in Eq. (B7) (solid line)

is verified in Supplementary Fig. 2. It follows that if $\mathcal{Z}_-(x) \sim 1 - Cx^{-1-\theta}$ for $x \to \infty$, then $\mathcal{G}_-(y) \sim y^{1+\theta}$ for $y \to 0$, which is here observed for all $d \geq 3$ (Supplementary Fig. 2). When SS approach jamming from above, the interaction potential gives $f = 2(\sigma - r)$ for $0 \leq r \leq \sigma$ and zero otherwise, so $G(f) = 1 - \frac{Z(\sigma - f/2)}{Z(\sigma)}$. In the jamming limit $G(2y\,\varepsilon\,\sigma) \to \mathcal{G}_+(y) = 1 - \mathcal{Z}_+(y)$, and therefore $\mathcal{G}_+(y) \sim y^{1+\theta}$, as in the previous case. This behavior is here observed in all $d \geq 3$ (Supplementary Fig. 2).

3. High d Structure

In the contact regime $r - \sigma \sim \Delta\varphi$, G-RT predicts that scaling functions $\mathcal{Z}_\pm^{\rm RT}$ should describe the growth of $Z(r)$ from 0 to the isostatic value, as given in Eqs. (C10) and (C17). Both results are tested in Supplementary Fig. 3 for d=3–10. The collapse is remarkably good for all x. The agreement with the G-RT scaling form is also remarkable for small x, but start to deviate from the theoretical prediction when $Z(r)$ approaches the isostatic $\bar{z} \approx 2d$ plateau. The type of deviation is different from each protocol, but is similar from one dimension to the next for a given protocol. For larger x in the near-contact region, the two protocols robustly produce the same power-law growth, $Z(r) \sim (r - \sigma)^{1-\alpha}$ with $\alpha \sim 0.40(1)$ (Supplementary Fig. 3), which is not predicted by G-RT. Because the number of rattlers vanishes with dimension neither of these phenomena can be ascribed to their presence. But because G-RT predictions rely on the individual cages to be Gaussian, which presumably they are not [8–10], it is natural to ascribe the discrepancy to the breakdown of that assumption.

At very large distances, the pair correlation function of any disordered systems trivially has $g(r \gg \sigma) = 1$, which corresponds to $Z(r \gg 1) \approx 2^d\varphi[(r/\sigma)^d - 1]$. Unsurprisingly this scaling form captures well the behavior of $Z(r)$ for both protocols and all d at large r, but the range of validity also extends with d (Supplementary Fig. 3). In order to quantify this effect, we fit the curves of $Z(r)$ for $r > \sigma$ using the form

$$Z(r) = C'(r - \sigma)^{1-\alpha} + 2^d\varphi[(r/\sigma)^d - 1)] \ . \qquad \text{(B8)}$$

When d grows, the region where the second term is much bigger than the first is

$$C'(r - \sigma)^{1-\alpha} < 2^d\varphi[(r/\sigma)^d - 1) \sim d\,2^d\varphi(r - \sigma)/\sigma \quad \text{(B9)}$$

hence $(r - \sigma) > [\sigma\, C'/(d\,2^d\varphi)]^{1/\alpha}$. The fitted values of C' indicate that the crossover point indeed decreases slowly with d.

APPENDIX C: REPLICA THEORY CALCULATIONS

The predictions of G-RT presented in this work are based on earlier results [7, 11]. Yet because the calculations in Ref. [7] have only been explicitly carried out for $d = 3$, and because different observables are considered, additional results are here presented. They are reported in this section and incidentally provide a somehow simplified derivation of the results of Ref. [7]. Nonetheless, reading this section requires a detailed knowledge of Refs [7, 11], so the reader who is not interested in the theoretical details can safely skip it. Note that as in the main text, this section uses reduced units $\epsilon = 1$ and $\sigma = 1$.

1. General expressions

The approximation scheme used is based on [7, Eq. (22) and (23)], which give the replicated free entropy separated between the harmonic and the liquid contributions

$$\begin{aligned}\mathcal{S}(m, A; T, \varphi) &= S_h(m, A) + \mathcal{S}_{\rm liq}(T/m, \varphi) \\ &\quad + 2^{d-1}\varphi y_{\rm liq}^{\rm HS}(\varphi) G(m, A; T) \ , \text{with} \\ G(m, A; T) &= d \int_0^\infty dr\, r^{d-1}\, [q(A, T; r)^m - e^{-\beta m v(r)}]\end{aligned} \qquad \text{(C1)}$$

for m replicas at temperature T, in a Gaussian cage of variance $2A$. The function $q(A, T; r) = \int d^d r' \gamma_{2A}(\vec{r}') e^{-\beta v(|\vec{r} - \vec{r}'|)}$ is defined in [7, just after Eq. (16)] where γ_{2A} is a normalized and centered Gaussian of variance $2A$, and $y_{\rm liq}^{\rm HS}$ is the HS cavity function. Introducing bipolar coordinates, as in [11, Appendix C.2.a], we obtain the generalization of [11, Eq. (C16)]

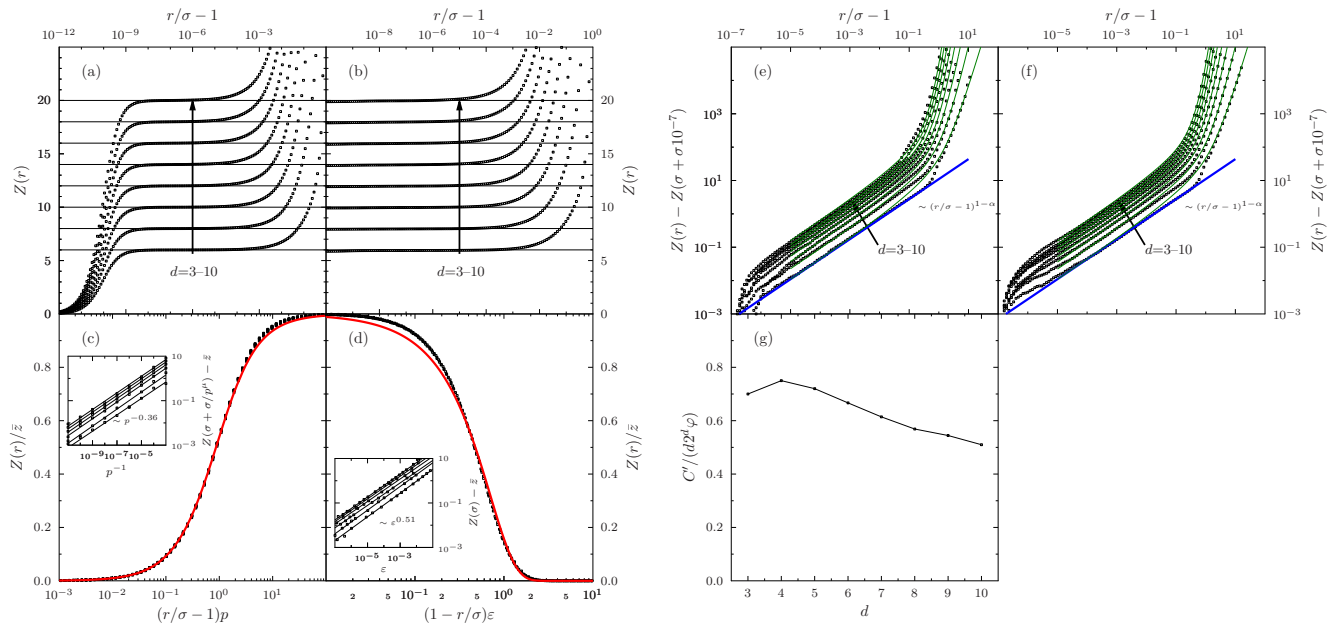

Supplementary Figure 3: Growth of the isostaticity $\bar{z} \sim 2d$ (solid lines) plateau with d=3–10 for **(a)** HS at $p = 10^{10}$ and **(b)** SS at $e \sim 10^{-20}$. The HS-SS contact regime **(c)-(d)** collapses remarkably well for all d, and the G-RT predictions (red line) are similarly accurate as in $d = 3$. The plateau height also consistently decay from d=3 to 8 (insets). **(e)-(f)** The HS-SS quasi-contact power-law growth is also robustly conserved, with a constant $\alpha = 0.42(2)$ (blue line). The fit to Eq. (B8) is also provided (green line). **(g)** The quasi-contact coefficient C' is such that the region where this regime can be observed shrinks with increasing d.

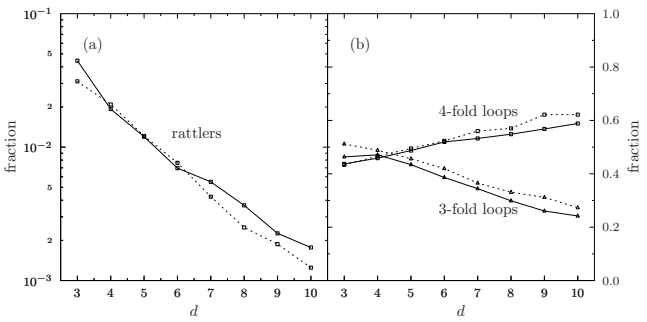

Supplementary Figure 4: **(a)** Fraction of rattlers in HS compressions (dashed line) and in SS energy minimizations from above (solid line). The fraction of particles left outside of the force network, the rattlers, also vanish with increasing d. For both protocols, the results suggest their fraction disappears exponentially with d. **(b)** Diminishing fraction of 3-member force loops (triangle) and growing fraction of 4-member force loops (square) with d for the two protocols. The force network, which is another observable for comparing the jammed packings, supports their structural similarity. The length of the force loops is also a simple measure of structural correlations. In the mean-field high d limit these loops are expected to become increasingly large, as the structural correlations vanish. The decrease in the fraction of 3-member loops and the growth of the fraction of 4-member loops, accompanied by a constant growth of the average length of the loops, is consistent with this scenario.

to the soft sphere potential $v(r) = (1-r)^2\theta(1-r)$

$$q(A,T;r) = \int_0^\infty du\, e^{-\beta v(u)} \left(\frac{u}{r}\right)^{\frac{d-1}{2}} \frac{e^{-\frac{(r-u)^2}{4A}}}{\sqrt{4\pi A}} \times \\ \times \left[e^{-\frac{ru}{2A}} \sqrt{\pi \frac{ru}{A}} I_{\frac{d-2}{2}}\left(\frac{ru}{2A}\right)\right] . \tag{C2}$$

The above equations (C1) and (C2) are the starting point of all the needed replica calculations for our analysis, and because we focus on the "jamming limit" of these equations, we take $T \to 0$ with $\tau = T/m$ and $\alpha = A/m$ held constant [7]. In Ref. [7] this limit was taken using a simplified form of Eq. (C2) for $d = 3$, but we here generalize the calculation to arbitrary d. The crucial observation [11, Eq. (C21)] is that when $z \to \infty$, $e^{-z}\sqrt{2\pi z} I_n(z) \to 1$. In the jamming limit the term in the second line of Eq. (C2) therefore disappears, because $A \to 0$ while r and u are of order 1. The remaining integral can then be evaluated via the saddle point approximation, because both β and $1/A$ diverge. Consider first the case $r < 1$. Assuming that the saddle point $u^* < 1$, one has to maximize the function $-\beta(1-u)^2 - (r-u)^2/(4A)$ which consistently maximizes $u^* = (4\beta A + r)/(1 + 4\beta A) = (4\alpha + \tau r)/(4\alpha + \tau) < 1$. Consider next the case $r > 1$. Assuming that in this case $u^* > 1$, we have $v(u) = 0$ and we thus consistently find $u^* = r > 1$. Replacing these expressions for u^* in

Eq. (C2) and taking the jamming limit we obtain

$$q(A,T;r)^m \to e^{-\frac{(1-r)^2}{4\alpha+\tau}\theta(1-r)} \ , \tag{C3}$$

and Eq. (C1) reduces to

$$\begin{aligned} \mathcal{S}_0(\alpha,\tau;\varphi) &= -\frac{d}{2}[\log(2\pi\alpha)+1] + \mathcal{S}_{\rm liq}(\tau,\varphi) \\ &\quad + 2^{d-1}\varphi y_{\rm liq}^{\rm HS}(\varphi) G_0(\alpha,\tau) \ , \\ G_0(\alpha,\tau) &= d\int_0^1 dr\, r^{d-1}\,[e^{-\frac{(1-r)^2}{4\alpha+\tau}} - e^{-\frac{(1-r)^2}{\tau}}] \ , \end{aligned} \tag{C4}$$

which replaces [7, Eqs. (D3) and (D4)].

The approach to jamming from above is described by the small τ limit [7, Appendix D.2]. In this limit we can consider the SS Mayer function as a small perturbation of the HS one and use standard liquid perturbation theory to write

$$\mathcal{S}_{\rm liq}(\tau,\varphi) = \mathcal{S}_{\rm liq}^{\rm HS}(\varphi) + d\, 2^{d-1}\varphi y_{\rm liq}^{\rm HS}(\varphi)\int_0^1 dr\, r^{d-1} e^{-(1-r)^2/\tau} \ . \tag{C5}$$

Plugging this result in Eq. (C4) we then get

$$\begin{aligned} \mathcal{S}_0(\alpha,\tau;\varphi) &= -\frac{d}{2}[\log(2\pi\alpha)+1] + \mathcal{S}_{\rm liq}^{\rm HS}(\varphi) \\ &\quad + 2^{d-1}\varphi y_{\rm liq}^{\rm HS}(\varphi) d\int_0^1 dr\, r^{d-1}\, e^{-\frac{(1-r)^2}{4\alpha+\tau}} \ . \end{aligned} \tag{C6}$$

Note *en passant* that the cancellation of the second term in Eq. (C5) with a corresponding term in $G_0(\alpha,\tau)$ is not surprising, as stated in [7, Appendix D.2], but has a deep physical interpretation. Indeed, Eq. (C4) shows that the "bare" SS potential $e^{-(1-r)^2/\tau}$ is modified around jamming by the presence of $m-1$ additional replicas (with $m\to 0$) that "renormalize" it to $e^{-(1-r)^2/(4\alpha+\tau)}$, as obtained in Eq. (C3). The crucial point is that the latter potential does not have a singularity when $\tau \to 0$, ensuring a smooth crossover and appropriate scalings around jamming.

2. The energy prefactor

Starting from Eq. (C6) and repeating the calculations of Ref. [7, Appendix D.2], we finally obtain the quadratic scaling of the energy as a function of $\Delta\varphi$ when approaching jamming from above. The general expression for the prefactor is then easily obtained. A further simplification is obtained by assuming that α is small at the jamming point, and developing the resulting expressions in powers of $\sqrt{\alpha}$ [11]. Doing so and optimizing over α and τ, one finally obtains

$$\begin{aligned} \sqrt{\alpha(\varphi)} &= \frac{1}{2^d\varphi y_{\rm liq}^{\rm HS}(\varphi)}\sqrt{\frac{4}{\pi}} \ , \\ \Sigma_0^{\rm HS}(\varphi) &= -d\log\left(\frac{\sqrt{8}}{2^d\varphi y_{\rm liq}^{\rm HS}(\varphi)}\right) + \frac{d}{2} + \mathcal{S}_{\rm liq}^{\rm HS}(\varphi) \ , \\ \mathcal{S}_1(\varphi) &= \frac{d\,\pi}{32}[2^d\varphi y_{\rm liq}^{\rm HS}(\varphi)]^2 \ , \\ \tau(\varphi) &= -\Sigma_0^{\rm HS}(\varphi)/(2\mathcal{S}_1(\varphi)) \ , \\ e(\varphi) &= [\Sigma_0^{\rm HS}(\varphi)]^2/(4\mathcal{S}_1(\varphi)) = d\,\tau^2/(8\alpha) \ . \end{aligned} \tag{C7}$$

The second line recovers the result of Ref. [11, Eq. (77)]. The glass close packing point $\varphi_{\rm GCP}$ [11], which is defined by the complexity $\Sigma_0^{\rm HS}(\varphi)=0$, is reported in Fig. 1. The first line shows that $\sqrt{\alpha(\varphi_{\rm GCP})}$ is indeed very small, being ~ 0.01 in $d=3$ and decreasing with dimension. Linearizing the last line around $\varphi_{\rm GCP}$ and using that $\Sigma_0^{\rm HS}(\varphi)$ vanishes linearly, one obtains the quadratic scaling of the energy and its prefactor [7]. G-RT results in Supplementary Fig. 1 have been obtained from this procedure, using the Carnahan-Starling equation of state in d dimensions for the HS liquid [11, Eq. (82)].

A last remark on the energy prefactor is in order. G-RT results in a discrepancy between the pressure computed from thermodynamics and that computed from the structural (see Refs. [11, Eq. (89)] and [7, Section VII.B]). This difference might have its origin in the fact that only two-body effective replica interactions are kept in this treatment. Indeed in the limit $d\to\infty$, where this approximation should be exact, the discrepancy disappears. It has also been observed in Ref. [7, Section VI.B] that a much better agreement between theory and numerical data is obtained if the distance from jamming $\Delta\varphi$ is corrected to account for this discrepancy. The correction factor obtained from the theory corresponds to the factor needed to impose the equality in [11, Eq. (89)], so rescaling $\Delta\varphi$ is equivalent to rescaling e_0. The rescaled predictions are also reported in Supplementary Fig. 1.

3. Scaling functions

To complete the analysis we compute the scaling functions $\mathcal{Z}_\pm(x)$ predicted by G-RT. Consider first the HS case, approaching jamming from below. The contact peak of $g(r)$ on approaching jamming is given by [11, Eq. (90)]

$$\begin{aligned} g(r) &= g(1)\Delta_0\left(2^{d-1}\varphi g(1)\frac{\sqrt{\pi}}{2}(r-1)\right) \\ &= \frac{p}{2^{d-1}\varphi}\Delta_0\left(p\frac{\sqrt{\pi}}{2}(r-1)\right) \ , \end{aligned} \tag{C8}$$

where $\Delta_0(x) = 1-\sqrt{\pi}xe^{x^2}[1-\mathrm{erf}(x)]$. The validity of the thermodynamic relation $p = 1+2^{d-1}\varphi g(1)$ is here assumed. As we discussed above, this relation is violated

by the theory, but the correction is here unimportant. If one does not want to use this relation, it is sufficient to replace $p \to 2^{d-1}\varphi g(1)$, but in the end this substitution does not affect the prediction for the scaling function.

Integrating Eq. (C8) using Eq. 1 from the main text we get, after changing the variable to $y = p\frac{\sqrt{\pi}}{2}(s-1)$

$$\begin{aligned} Z(r) &= 2d\,p\int_1^r ds\, s^{d-1}\,\Delta_0\left(p\frac{\sqrt{\pi}}{2}(s-1)\right) \\ &= 2d\frac{2}{\sqrt{\pi}}\int_0^{p\frac{\sqrt{\pi}}{2}(r-1)} dy\,\left[1+\frac{y}{p}\frac{2}{\sqrt{\pi}}\right]^{d-1}\Delta_0(y)\ . \end{aligned} \tag{C9}$$

We notice now that $p \sim 1/\Delta\varphi$ and $r-1 \sim \Delta\varphi$. The integration is therefore over an interval of order 1. The first term in the integrand can be neglected because for y of order 1, so this term goes to 1 when $\Delta\varphi \to 0$. Finally we obtain in the contact region

$$\begin{aligned} \frac{Z(r)}{2d} &= \frac{2}{\sqrt{\pi}}\int_0^{\frac{\sqrt{\pi}}{2}x} dy\Delta_0(y) \\ &= 1-e^{\frac{\pi}{2}x^2}\left[1-\mathrm{erf}\left(\frac{\sqrt{\pi}}{2}x\right)\right] \equiv \mathcal{Z}_-^{\mathrm{RT}}(x)\ , \end{aligned} \tag{C10}$$

where $x = p(r-1)$. This prediction is tested in Fig. 3 of the main text and in Supplementary Fig. 3.

Next consider the SS case approaching jamming from above, working in the jamming limit. $T \to 0$ with $\tau = T/m$ and $\alpha = A/m$. In this case the calculation starts from [7, Eqs. (17) and (48)]. Using bipolar coordinates we can write

$$\begin{aligned} \frac{g(r)}{y_{\mathrm{liq}}^{\mathrm{HS}}(\varphi)} &= e^{-\beta v(r)}\int_0^\infty du\, q(A,T;u)^{m-1}\left(\frac{u}{r}\right)^{\frac{d-1}{2}}\times \\ &\times\frac{e^{-\frac{(r-u)^2}{4A}}}{\sqrt{4\pi A}}\left[e^{-\frac{ru}{2A}}\sqrt{\pi\frac{ru}{A}}I_{\frac{d-2}{2}}\left(\frac{ru}{2A}\right)\right]\ . \end{aligned} \tag{C11}$$

We now need to improve Eq. (C3) by considering the quadratic corrections around the saddle point, which for $r<1$ leads to

$$q(A,T;r) \sim e^{-\frac{(1-r)^2}{m(4\alpha+\tau)}}\left[\frac{4\alpha+\tau r}{r(4\alpha+\tau)}\right]^{\frac{d-1}{2}}\frac{1}{\sqrt{1+4\alpha/\tau}}\ . \tag{C12}$$

Plugging Eq. (C12) in Eq. (C11), dropping as before the last term in square brackets in Eq. (C11), and evaluating the integral via the saddle point approximation including quadratic corrections, we find for $r<1$ that

$$\begin{aligned} \frac{g(r)}{y_{\mathrm{liq}}^{\mathrm{HS}}(\varphi)} &= e^{-\frac{4\alpha+\tau}{\tau^2}(r-1)^2}\left(1+\frac{4\alpha}{\tau}\right)\times \\ &\times\left[\frac{1}{r}\left(1+(r-1)\left(1+\frac{4\alpha}{\tau}\right)\right)\right]^{d-1}\times \\ &\times\theta\left(1+(r-1)\left(1+\frac{4\alpha}{\tau}\right)\right)\ . \end{aligned} \tag{C13}$$

Plugging this result in Eq. (1), and assuming that we approach jamming from above, so that $\tau \ll 4\alpha$, we obtain for $r > \frac{4\alpha}{\tau+4\alpha} \sim 1-\frac{\tau}{4\alpha}$ that

$$\begin{aligned} Z(r) &= y_{\mathrm{liq}}^{\mathrm{HS}}(\varphi)d\,2^d\varphi\frac{4\alpha}{\tau}\int_{1-\frac{\tau}{4\alpha}}^r ds\, s^{d-1}\times \\ &\times\left[\frac{1}{s}\left(1+(s-1)\frac{4\alpha}{\tau}\right)\right]^{d-1} e^{-\frac{4\alpha}{\tau^2}(s-1)^2}\ . \end{aligned} \tag{C14}$$

Changing variables to $y = (1-s)\frac{4\alpha}{\tau}$ and using the first line of Eq. (C7) gives

$$Z(r) = d\sqrt{\frac{4}{\pi\alpha}}\int_{(1-r)\frac{4\alpha}{\tau}}^1 dy\,(1-y)^{d-1}e^{-\frac{y^2}{4\alpha}}\ . \tag{C15}$$

Although this result is already the desired scaling function, we can further simplify it by noting that α is small to write

$$\begin{aligned} Z(r) &= d\sqrt{\frac{4}{\pi\alpha}}\int_{(1-r)\frac{4\alpha}{\tau}}^\infty dy e^{-\frac{y^2}{4\alpha}} \\ &= 2d\left[1-\mathrm{erf}\left(\frac{2\sqrt{\alpha}}{\tau}(1-r)\right)\right] \\ &= 2d\left[1-\mathrm{erf}\left(\sqrt{\frac{d}{2e}}(1-r)\right)\right]\ , \end{aligned} \tag{C16}$$

where in the last line we used the last line of Eq. (C7). The resulting prediction

$$\mathcal{Z}_+^{\mathrm{RT}} = 1-\mathrm{erf}(x) \tag{C17}$$

is tested in Fig. 3 of the main text and in Supplementary Fig. 3.

[1] H. L. Frisch and J. K. Percus, Phys. Rev. E **60**, 2942 (1999).
[2] M. Skoge, A. Donev, F. H. Stillinger, and S. Torquato, Phys. Rev. E **74**, 041127 (2006).
[3] S. Torquato and F. H. Stillinger, Rev. Mod. Phys. **82**, 2633 (2010).
[4] P. Charbonneau, A. Ikeda, G. Parisi, and F. Zamponi, Phys. Rev. Lett. **107**, 185702 (2011).
[5] A. Donev, S. Torquato, and F. H. Stillinger, Phys. Rev. E **71**, 011105 (2005).
[6] J. A. van Meel, B. Charbonneau, A. Fortini, and P. Charbonneau, Phys. Rev. E **80**, 061110 (2009).
[7] L. Berthier, H. Jacquin, and F. Zamponi, Phys. Rev. E **84**, 051103 (2011).

[8] P. Chaudhuri, L. Berthier, and S. Sastry, Phys. Rev. Lett. **104**, 165701 (2010).
[9] F. Lechenault, R. Candelier, O. Dauchot, J.-P. Bouchaud, and G. Biroli, Soft Matter **6**, 3059 (2010).
[10] P. Charbonneau, A. Ikeda, G. Parisi, and F. Zamponi, Proc. Nat. Acad. Sci. U.S.A. **139**, 13939 (2012).
[11] G. Parisi and F. Zamponi, Rev. Mod. Phys. **82**, 789 (2010).